CEAS Aeronautical Journal (2019) 10:431–442
https://doi.org/10.1007/s13272-018-0325-0

ORIGINAL PAPER

Multidisciplinary analysis of subsonic stealth unmanned combat aerial vehicles

E. Sepulveda[1] · H. Smith[1] · D. Sziroczak[1]

Received: 8 March 2018 / Accepted: 28 August 2018 / Published online: 1 September 2018
© The Author(s) 2018

Abstract
In this paper, the GENUS multidisciplinary aircraft design and analysis environment is presented in its application to the conceptual design of tailless, low-observable unmanned combat aerial vehicles (UCAVs). Analysis disciplines comprise a variety of low to medium fidelity, physics-based and empirical methodologies, as well as higher order panel method aerodynamic analysis. Stealth considerations have been included in terms of a radar cross section analysis through a physical optics approximation method, with results verified against a well-known radar cross section prediction code. Preliminary results show good agreement for gross and empty masses when compared to several existing UCAV demonstrators and conceptual designs. A further validation of the presented methodologies is evaluated through the design, analysis, and optimisation of an unmanned strike fighter concept.

Keywords UCAV · Stealth · Conceptual design · Tailless aircraft · UAV

1 Introduction

Aircraft conceptual design consists of balancing the trade-offs and constraints imposed by various disciplines and mission requirements. This battle intensifies as the aircraft's role becomes more demanding, such as the case for multirole aircraft.

During these early design stages, the freedom of configuration, systems, and subsystems is greater and will have a significant impact on the overall cost and complexity of the project. It is vital, therefore, to correctly identify the major design parameters and their interactions in the most integrated way possible.

This is achieved to a certain degree through the use of multidisciplinary design analysis and optimisation (MDAO) tools and their integration into computational systems. MDAO has been extensively used in aircraft conceptual, system, and subsystem design, as well as in numerous other engineering disciplines [1, 2].

✉ E. Sepulveda
e.sepulveda@cranfield.ac.uk

H. Smith
howard.smith@cranfield.ac.uk

[1] School of Aerospace, Transport and Manufacturing, Cranfield University, Cranfield, Beds MK43 0AL, UK

During the initial design stages, well established yet simple empirical and semi-empirical analysis techniques are commonly employed; such techniques are readily available in many aircraft design textbooks and references, and they represent the lowest level of fidelity [3–5]. Variable fidelity MDAO frameworks aim to replace such empirical methods with physics-based analysis tools, response surfaces based on experimental data, and even high fidelity tools such as computational fluid dynamics (CFD) and finite element analysis (FEA) [6–9].

2 GENUS aircraft design environment

The GENUS aircraft design environment [10] has been under development in Cranfield University's Aircraft Design Group since the year 2012. Its name derives from the taxonomical classification of biological organisms, and it represents the capability of the framework to model and analyse different species of aircraft under a common framework. GENUS is a Java-based architecture, and consists of nine essential modules; namely geometry, mission, propulsion specification, mass breakdown, aerodynamics, propulsion analysis, packaging, performance, and stability. Special modules can be added to suit the needs of the particular aircraft designs. Furthermore, a gradient-based, and a

custom-made genetic algorithm can be used in multivariate, single objective optimisation.

The methodologies currently integrated into the GENUS environment allow the design and analysis of civil transport aircraft [11], blended wing body transport aircraft [12], hypersonic launch vehicles [13], solar-powered high-aspect-ratio UAVs [14], and supersonic business jets [15].

3 UCAV design and analysis

UCAV design involves a higher integration of multiple aircraft design disciplines from the earliest design stages. This is due to the dominance of stealth and high-performance constraints and requirements. The main technological challenges behind stealth UCAV design involve complex aerodynamics, packaging, and the effects of integrating low-observability into a balanced design [16].

3.1 Geometry

A fully parametric geometry is created via body components, and lifting surfaces. The complete geometry input is defined in Table 1. This module provides great flexibility to the designer using simple shape definitions. Body component sections contain simple primitives such as an oval and a square, while lifting surfaces have NACA 4 series, NACA 5 series, NACA 6 series, wedge, double wedge, and biconvex aerofoils as available input options.

Furthermore, different geometry formats, such as XYZ point-cloud, and LAWGS [17], are applied to link the geometry input to various analysis disciplines, such as aerodynamics, packaging, and sonic boom prediction. Figure 1 shows GENUS' geometry module flexibility.

3.2 Mission

The mission module serves only as inputs for other analysis modules. The mission is defined by estimated take-off mass, target range, cruise Mach or speed, cruise altitude, loiter time and altitude, payload, droppable, and retrievable payload. Additional inputs can complete different types of mission, such as ground strike, reconnaissance, etc.

3.3 Propulsion specification and analysis

This module consists wholly of engine type, number of engines of each type, engine design point and limits, as well as type of fuel and storage (internal or external). This information is used by the propulsion analysis module to obtain engine performance over a wide range of operational conditions.

Table 1 Parametric geometry elements in GENUS

Geometry component	Classes	Defining parameters
Body component	Fuselage Nacelle Tail boom External fuel tank	XYZ Apex, number of sections, cross section shape, section dimensions, section apex, and master component
Lifting surface	Wing Vertical tail Horizontal tail Canard	XYZ apex, and number of sections; each section is defined by Aerofoil Span Root chord Tip chord Root incidence Twist Sweep Dihedral

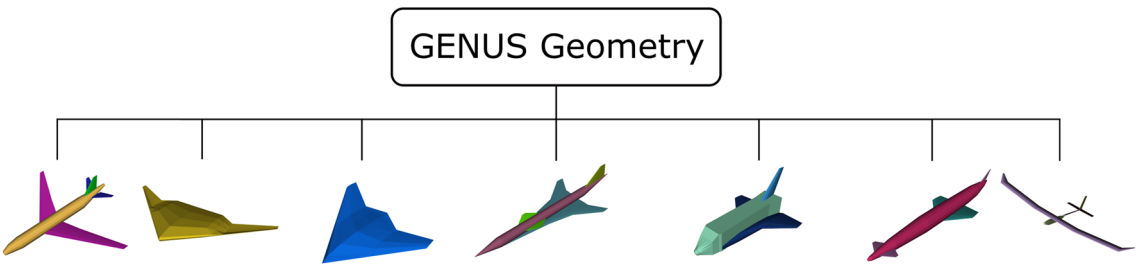


Fig. 1 GENUS geometry representation of various aircraft species

The lowest fidelity models include semi-empirical regression equations such as those presented by Raymer [5, Chap. 13] and Howe [3, Chap. 3.6] for turbojet/turbofan engines. On a higher fidelity level, a thermodynamic analysis of turbojet, turbofan, and ramjet engines has been adapted from the NASA open source java applet EngineSim [18]. Material and fuel type selections are also available through this code.

Figure 2 shows EngineSim results compared to data from a GE J79-10B engine in dry mode at various altitudes, Mach numbers, and throttle settings [19]. Results show good agreement for the conceptual design stage.

3.4 Mass breakdown

The mass build-up of novel configurations often relies on a combined approach, where methodologies for similar classes of aircraft are employed. UCAV mass breakdown makes use of system and structure mass estimations by Gundlach [20], Raymer [5], Roskam [21] and in-house methods [22]. These methodologies are design sensitive rather than merely statistical. Modern materials and manufacturing techniques can be accounted via 'technology reduction factors'. These factors also allow the performing of sensitivity studies on the impact of future technologies applied to UCAV designs.

Mass breakdown results for several UCAV demonstrators and available conceptual designs show good agreement in terms of gross and empty masses, as shown in Fig. 3. The empty mass of the Taranis UCAV resulted from an educated guess and comparison to similar designs. A slight over-prediction in empty mass values can also be seen as a result from the use of manned fighter equations where methodologies specific for UCAVs are not available.

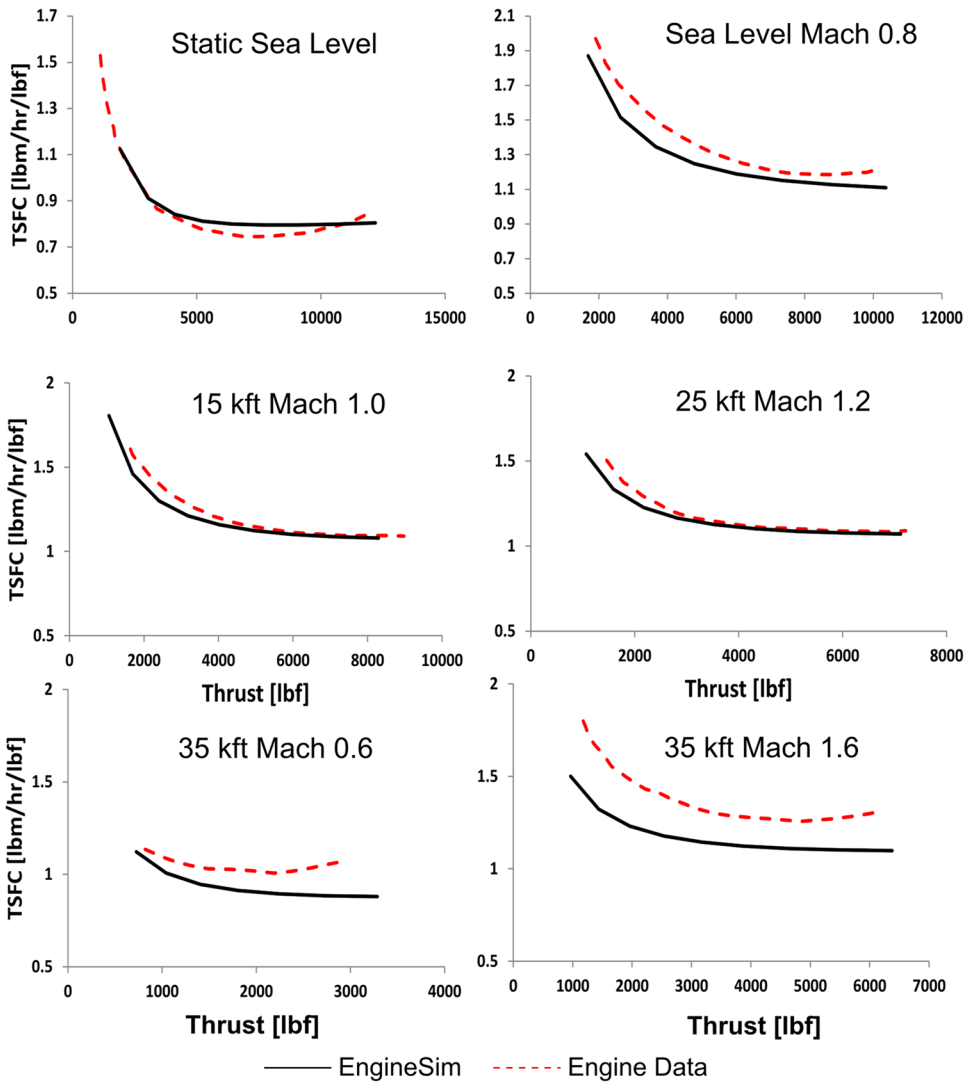


Fig. 2 Thrust and TSFC verification for a GE J79-10B engine in EngineSim

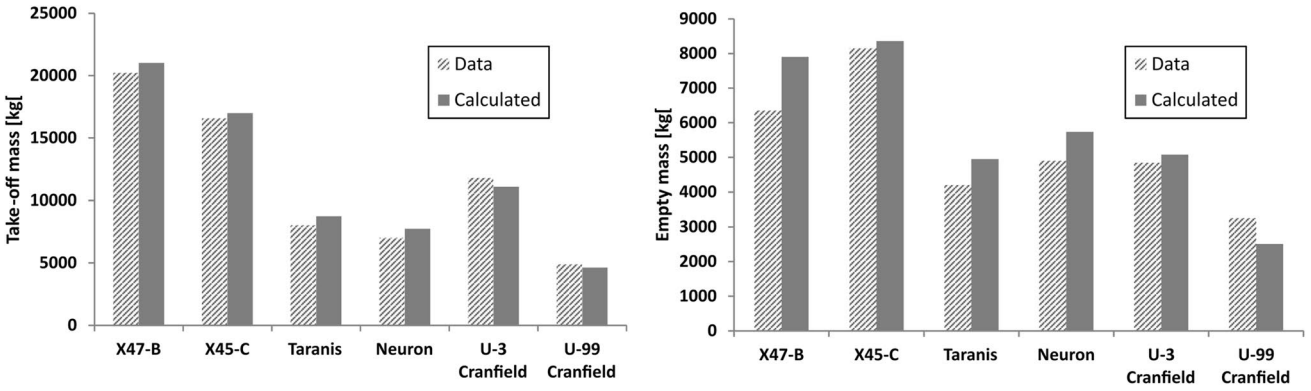


Fig. 3 Mass breakdown validation for various UCAVs

3.5 Aerodynamics

3.5.1 Zero-lift drag

Skin friction and form drag are obtained through the FRICTION code equations [23]. This allows for fully laminar, fully turbulent, or combined boundary layers. Total zero-lift drag is given by:

$$C_{D_0} = \sum_{i=1}^{N} \frac{FF_i S_{\text{wet}i} C_{Fi}}{S_{\text{ref}}} \tag{1}$$

The effects of boundary layer turbulence are included through a transition percentage F_{trans} as stated in the equation below:

$$C_{F_{\text{Total}}} = C_{F\text{turb}} - F_{\text{trans}}\left[C_{F\text{turb}} - C_{F\text{lam}}\right]. \tag{2}$$

3.5.2 Wave drag

When operating at speeds higher than the critical Mach number the effects of compressibility and local shock waves must be accounted for. The drag divergence Mach number (M_{DD}) is defined as the Mach number that causes an increase of 20 drag counts due to wave drag. M_{DD} can be estimated from the span-wise lift distribution through the following equation [24]:

$$M_{\text{DD}}\cos\Lambda_{0.5} + \frac{C_l(y)}{10\cos^2\Lambda_{0.5}} + \frac{t/c(y)}{\cos\Lambda_{0.5}} = K_{\text{Aerofoil}}, \tag{3}$$

where the value of K_{Aerofoil} ranges from 0.87 for normal aerofoils to 0.95 for supercritical and advanced aerofoils. The local critical Mach number and the wave drag increment on a wing strip are given by:

$$M_{\text{cr}} = M_{\text{DD}} - \sqrt[3]{\frac{0.1}{80}}, \tag{4}$$

$$C_{dw} = \begin{cases} 0, & M \leqslant M_{\text{cr}} \\ 20\left(M - M_{\text{cr}}\right)^4, & M > M_{\text{cr}} \end{cases}. \tag{5}$$

Finally, the total wave drag coefficient over the wing can be obtained by adding the contributions of individual wing strips via:

$$C_{dw} = \sum_{i=1}^{n} C_{dw_i} \frac{S_{\text{strip}_i}}{S_{\text{ref}}} \tag{6}$$

The drag rise behaviour and drag divergence Mach number for a delta wing UCAV at cruise altitude are shown in Fig. 4.

3.5.3 Panair aerodynamic analysis

The linear potential solver Panair [25] has been integrated into the GENUS framework for aerodynamic analyses. Panair uses a higher order panel method which solves the Prandtl–Glauert equation for subsonic and supersonic flows over arbitrary bodies, a distinct advantage from other panel methods. Panair provides forces, moments, and flow field

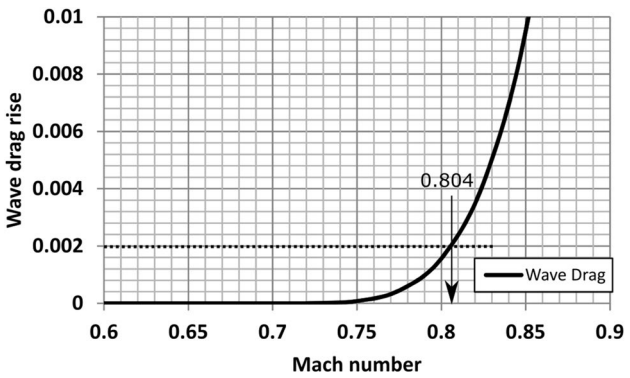


Fig. 4 Drag rise due to wave drag

information over the entire configuration as well as over user-defined cuts, planes, and off-body points; for a comprehensive explanation see the user's manual [26].

The FORTRAN-based Panair a502 solver has been linked to the GENUS Java framework via a JNI-C++ interface, which translates Java inputs into native code format. A C++ wrapper file then calls the appropriate FORTRAN subroutines, the results of which are then translated into Java data types via the same native link. The C++ and FORTRAN files are compiled into a dynamic library, which can be called directly from Java, Fig. 5, thus resulting in a faster execution time when compared to sequences that write to disk, as found in other frameworks.

A specific geometry format was developed to properly mesh the entire aircraft, which automatically assigns the correct network boundary conditions, wake edge attachment, and wake boundary condition to all components. Wings are meshed as thick lifting surfaces, while tail plane and canards are idealised as thin cambered surfaces. Fuselages are divided into sections depending on the number and location of lifting surfaces. An example of network division of a civil transport and a supersonic business jet are shown in Fig. 6. This format does not include bi-planes, box-wing aircraft, serpentine inlets, and body-mounted engine nacelles, such as those used for boundary layer ingestion.

Results of this process have been validated with flight data measurements for a 737-100 aircraft [27] (Fig. 7), and low speed wind tunnel data for UCAV 1303 [28] (Fig. 8). It can be seen that Panair cannot account for flow separation and vortex breakdown effects at moderate angles of attack for moderate to high sweep, low aspect ratio configurations. Thus, the validity of the pitching moment coefficient results is limited to moderate angles of attack.

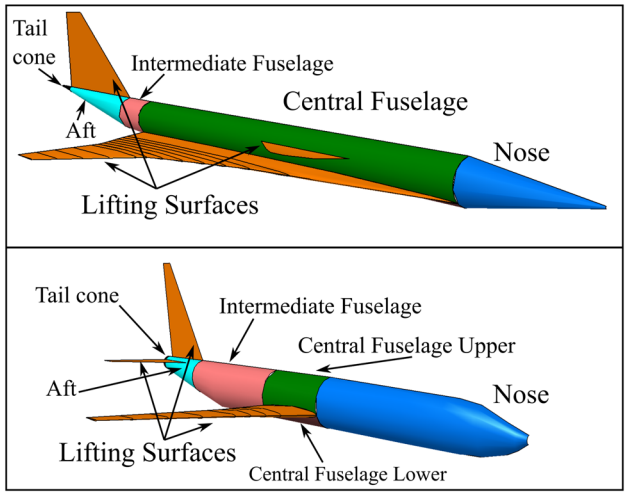


Fig. 6 Network divisions for supersonic business jet and conventional airliner

3.6 Packaging and centre of gravity

This module checks that the overall volume of the aircraft is sufficient to accommodate the internal components, such as particular types of payload, the propulsion system components, fuel tanks, avionics box, and landing gear.

The number of internal weapon bays depends on payload mass and type of weapon system, and their dimensions are determined following the sizing procedure given by Raymer [5]. Integral fuel tank volume is determined for wing segments through the differential volumes procedure shown in Fig. 9 below [29].

$$\Delta v = \frac{\Delta y}{6}\left[\Delta x_1\left(2\Delta z_1 + \Delta z_2\right) + \Delta x_2\left(\Delta z_1 + 2\Delta z_2\right)\right], \tag{7}$$

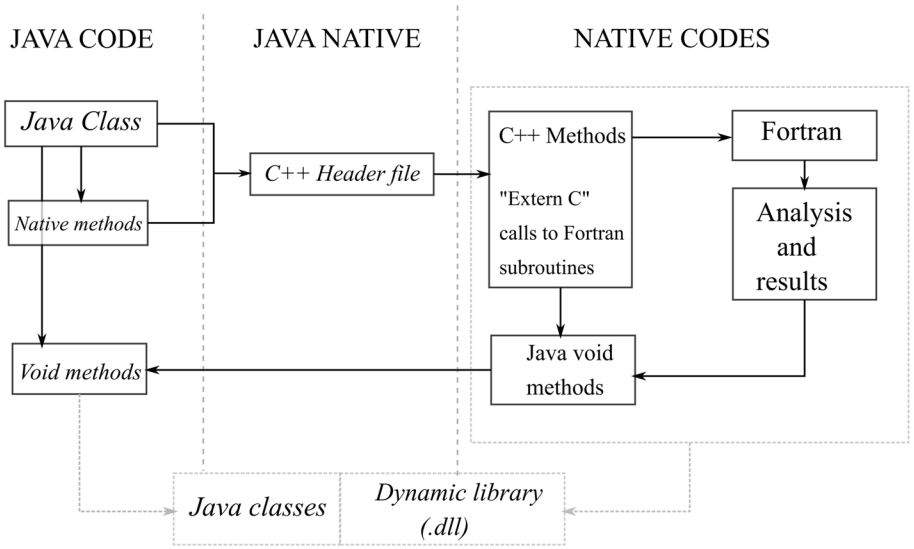


Fig. 5 Panair integration into the GENUS framework through JNI and C++ wrapper

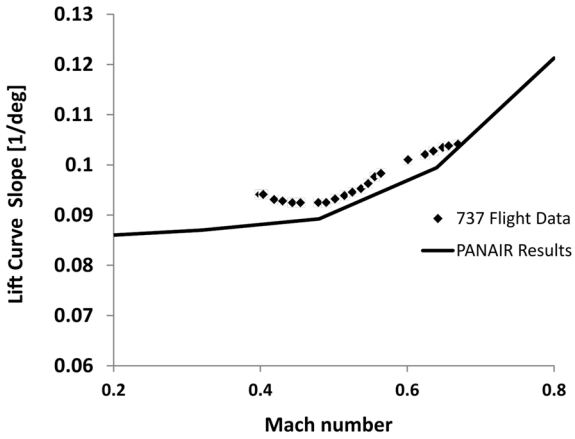


Fig. 7 PANAIR vs flight data: lift curve slope results for a Boeing 737-100

$$\Delta z_j = \frac{1}{2}(z'_j + z''_j). \tag{8}$$

Forward and rear fuel tank limits correspond to the position of wing front and rear spars, which are specified by the user by engineering judgement. The total volume is corrected by a factor less than 1 to account for the wing structural components. In the case that other components are located inside the wing fuel tanks, the corresponding volume of said components is subtracted. Figure 10 shows a packaged lambda-wing UCAV.

The location of the centre of gravity for each mass configuration is obtained through Eq. (9):

$$x_{\mathrm{CG}} = \frac{\sum_i x_i m_i}{m_i}. \tag{9}$$

Items can be handled in the longitudinal and lateral directions to comply with packaging or stability constraints by specifying a container shape, a relative CG position, and a master component.

3.7 Performance

Performance requirements are mostly specified in the 'Mission' module, but additional information, such as manoeuvres and field performance, can be included here. Ingress and egress segment specifications can also be added to analyse different missions, such as Hi–Lo–Hi.

Take-off performance has been adapted from Lynn's TAKEOFF2 code [30]. Normal take-off and balanced field length calculations are available, as well as thrust vectoring effects.

Landing performance is obtained via Eq. (10) [31, Chap. 5]:

$$s_L = \frac{1.69 W_L^2}{\rho S C_{L_{\max}} g[D + \mu(W_L - L)]_{0.7V_L}}. \tag{10}$$

Climb segments are optimised using ESDU 91016 [32] energy height optimisation to minimise time-to-climb or

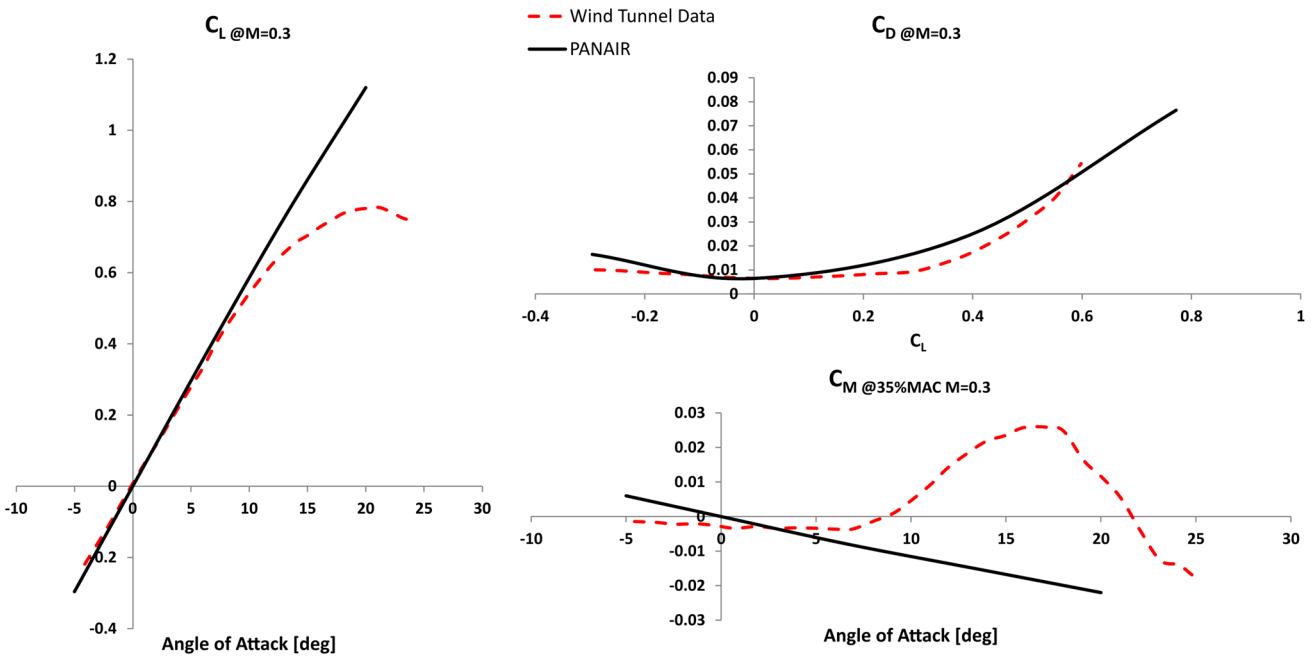


Fig. 8 UCAV 1303 wind tunnel data compared to PANAIR outputs

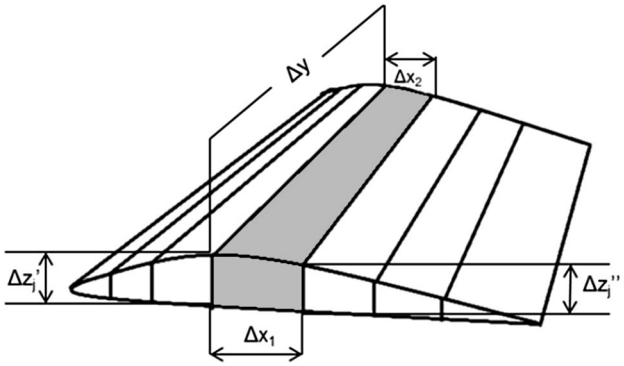


Fig. 9 Differential volumes in a wing segment between successive aerofoils

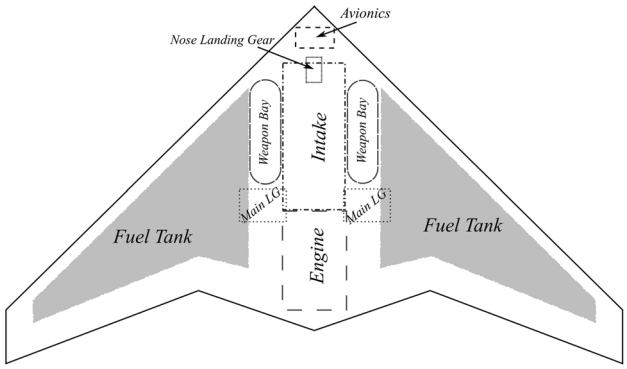


Fig. 10 X45-C type UCAV showing packaged components, top view

fuel-to-climb, as chosen by the user. The algorithm achieves the energy height given by a target Mach-altitude or speed-altitude point, after which a constant energy height climb/descent is performed as required.

Specific excess power is obtained from propulsion and aerodynamic results via Eq. (11):

$$P_S = V\left[\frac{T}{W} - \frac{qC_{D0}}{W/S} - n^2\frac{KW}{qS}\right]. \tag{11}$$

Cruise segments are evaluated through constant speed and altitude, constant altitude and attitude, or constant speed and attitude profiles [33, Chap. 20], the main output being the fuel consumption.

Achievable sustained turn rates are constrained through the required thrust as shown in Eq. (13), while instantaneous turn rate is constrained through the maximum wing loading obtained from Eq. (14):

$$\dot{\psi} = \frac{g\sqrt{n^2-1}}{V}, \tag{12}$$

$$D_{\text{SustTurn}} = T_{\text{Req}} = qC_{D_0}S + \frac{K\left(n_{ST}W\right)^2}{qS}, \tag{13}$$

$$(W/S)_{\max} = \frac{qC_{L_{\text{Usable}}}}{n_{\text{Inst}}k_{\text{mass}}}. \tag{14}$$

Acceleration requirements are also evaluated through specific excess power constraints assuming an average acceleration, Eq. (15):

$$P_{s\text{Req}} = \frac{V}{g}\left(\frac{V_{\text{final}} - V_{\text{inital}}}{\Delta t}\right). \tag{15}$$

3.8 Stability

USAF Digital Datcom has been fully integrated into the GENUS framework following the procedure shown for Panair, where geometric and flight condition inputs are automatically transformed into a Datcom specified format, as shown in Fig. 5.

Longitudinal and lateral static stability derivatives, as well as effects from symmetric flap-type control surfaces are extracted from the Datcom analysis modules, and used to calculate static margin and trim for all user-specified flight conditions. Longitudinal stability is constrained through the static margin for all flight conditions, where the static margin is defined as:

$$K_n = \frac{X_{np} - X_{CG}}{\bar{c}}. \tag{16}$$

For tailless aircraft, trim becomes problematic due to their short moment arm and coupled control surfaces. Following Castro's procedure [34], Eqs. (17)–(21), and with symmetric flap deflection results from Datcom, trim can be achieved through an angle of attack, and a control surface deflection:

$$\alpha_{\text{trim}} = \frac{C_K C_{L\delta e} - C_B C_{m\delta e}}{\text{Det}}, \tag{17}$$

$$\delta_{e\text{trim}} = \frac{C_B C_{m\alpha} - C_{L\alpha} C_K}{\text{Det}}, \tag{18}$$

$$\text{Det} = C_{L\delta e}C_{m\alpha} - C_{L\alpha}C_{m_{\delta e}}, \tag{19}$$

$$C_K = -C_{m0}, \tag{20}$$

$$C_B = C_{L\text{trim}} - C_{L0} \tag{21}$$

3.9 Special modules—radar cross section

Stealth constraints often dominate the design choices for UCAVs. One of the main parameters concerning low observability is radar cross section (RCS), which is a measure of the amount of energy reflected by a target in a particular direction when it is illuminated by electromagnetic waves. Monostatic RCS is defined in terms of the scattered and incident electric fields as:

$$\sigma = \lim_{r\to\infty} 4\pi r^2 \frac{|E_{\text{scat}}|^2}{|E_{\text{inc}}|^2}. \tag{22}$$

Numerical approximations to the RCS of a target have existed since the late 1980s [35]. POFACETS is a physical optics approximation Matlab®-based code that discretizes the geometry into triangular facets and computes the total signature by superposition of scattering resulting from the illuminated facets [36], including the effects of different materials and ground plane [37].

POFACETS routines have been translated into appropriate Java methods as part of a special module. Convex hulls and Delaunay triangulation routines are used to discretize the geometry [38]. Results in Fig. 11 show good agreement between the original code and the Java version for a clean lambda-wing UCAV using perfect electric conductor material and no ground plane effect.

4 Framework validation

The presented methodologies are evaluated through AIAA's unmanned strike fighter request for proposal (RFP) [39]. The relevant requirements are summarized in Table 2.

The design starting point consists of a lambda-wing UCAV geometry, which can be parametrised with the seven inputs shown in Fig. 12, with the addition of the aerofoil incidence angle at each wing station. NACA6 aerofoils are used through design process, with thicknesses varying across the span, from 15% at the centre to 10% at the tip. This initial design does not comply with several mission constraints.

The propulsion system is assumed to be a buried, central low-bypass turbofan. The payload has been divided into two internal weapon bays, each carrying one GBU-32 JDAM. Longitudinal control is achieved through elevons located in the first wing kink, with the chord ratio chosen as that to satisfy trim constraints for all flight conditions.

Table 3 shows the lower and upper bounds on the input variables, as well as the initial and final design points' characteristics.

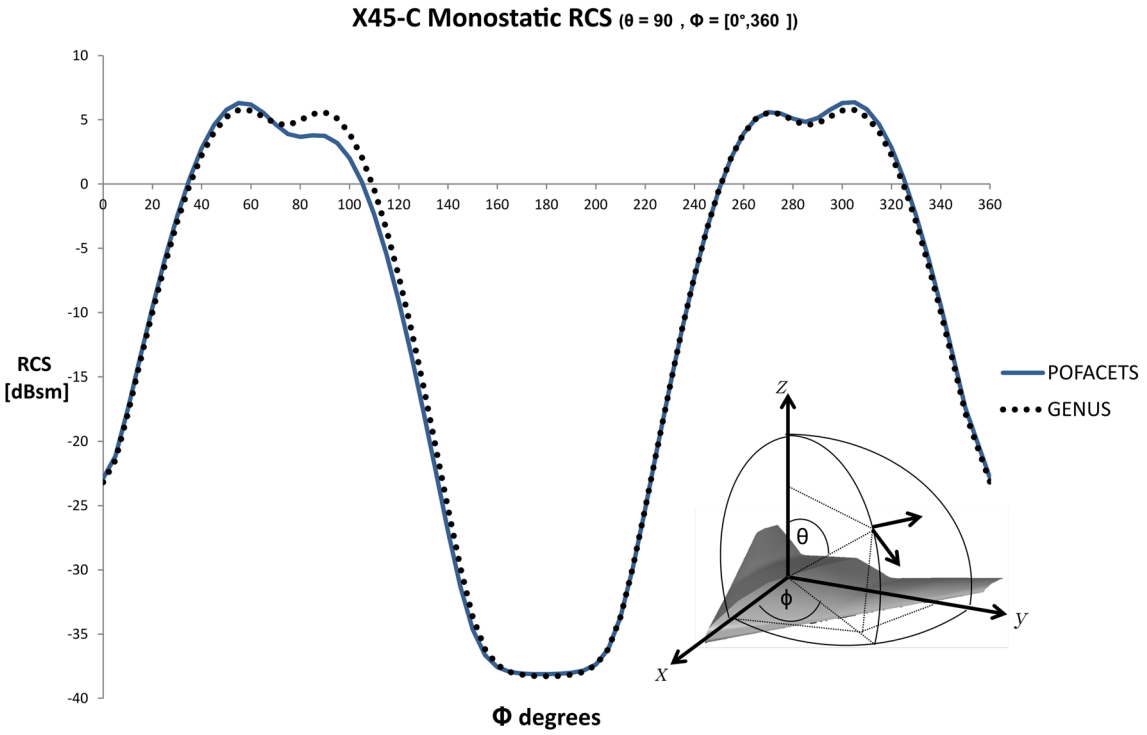


Fig. 11 Radar cross section comparison

Table 2 Unmanned strike fighter RFP

Payload	2000 lb JDAM
Range/performance	800 nm radius, cruise Mach ≥ 0.7 at 40,000+ ft with 1.5 turns mid-mission at cruise speed/alt., instant. turn rate ≥ 20°/s. Ingress/egress of 100 nm each at Mach 0.9 and 250 ft
Acceleration	$M = 0.4$–0.8 at 5000 ft. in 40 s
Specific excess power	> 200 ft/s at 5000 ft. and $M = 0.4$
Ferry range	3000 nm (external tanks allowed)
Take-off/landing	< 5000 ft
Propulsion	Off-the-shelf commercial jet engine
Signature	Low observables (RCS and IR) ~ set as < − 20 dBsm nose-on view S-band (~ 3 GHz)
Avionics	500 lb allowance for classified treatments avionics

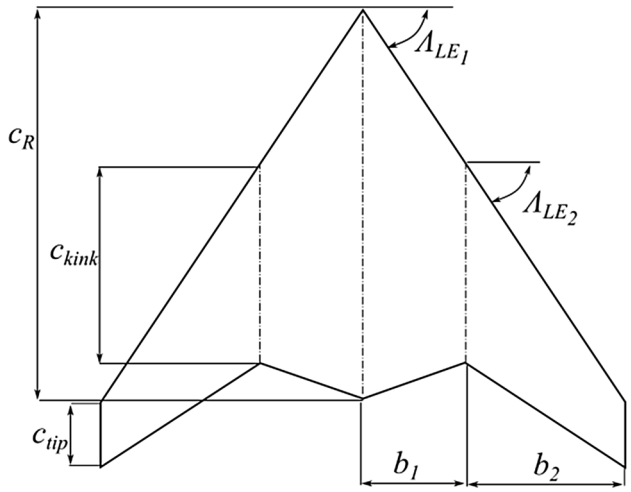


Fig. 12 Geometry input parameters, lambda wing UCAV

Figure 13 shows the top view comparison between the initial design point and the optimised configurations, overall length and wing span, as well as the location of the internal weapon bays.

It can be seen that the resulting configurations shows a significant improvement in the aerodynamic performance of the vehicle, which results in a smaller engine and consequently 25.2% less fuel required. The gross mass reduction is approximately 8%. Furthermore, an improvement in longitudinal stability is also observed, however the upper static margin limit was violated. Figure 14 shows mass and static margin profiles throughout the mission segments, the drag polar for both configurations at the cruise condition, as well as the mass breakdown.

Figure 15 shows the comparison of RCS signatures for both configurations, assuming perfect electric conductor as material. The integration of the RCS analysis into the optimisation loop, added with a library of radar absorbent materials is still in progress and will be the topic of a dedicated paper.

5 Conclusions

An aircraft design, analysis, and optimisation environment has been shown in its application to low observable unmanned combat aerial vehicles. The methodologies vary from empirical regressions to physics-based numerical solutions, with multiple fidelity levels included for various disciplines. The methodologies so far cover subsonic and low supersonic designs and missions, which are the most likely roles for UCAVs to perform in the near future.

Mass breakdown methods resulted in good agreement between UCAV quoted data and calculated maximum take-off mass and operating empty mass, while maintaining design sensitivity, and not purely statistical approximations.

The higher order panel method Panair has been efficiently integrated into the design environment to perform automatic aerodynamic analysis of arbitrary configurations for speed regimes up to Mach 4.0. Similarly, USAF digital Datcom performs automatic stability and control analysis for full configurations including longitudinal control surfaces such as elevons.

Low observability analysis is currently limited to monostatic radar cross section signatures of clean configurations. This analysis has been adapted from the well-known

Table 3 Unmanned strike fighter optimisation results

Design parameters	Lower bound	Upper bound	USF_0	USF_{Opt}
C_{Root} (m)	5	6.5	6	5.85
C_{Kink} (m)	2.5	3.8	3.6	3.8
C_{Tip} (m)	0.1	1	0.5	1
b_1 (m)	1	3	1.25	1.69
b_2 (m)	2.5	4	2.98	3.45
Λ_{LE1}	40°	65°	56.7°	55.7°
Λ_{LE2}	40°	65°	56.7°	53.6°
$Incidence_{Root}$	− 2°	2°	0°	2°
$Incidence_{Kink}$	− 2°	2°	0°	− 2
$Incidence_{Tip}$	− 3°	1°	0°	− 1.5°
MTOM (kg)	5500	7500	6758	6221
OEM (kg)			3601	3588
Fuel (kg)	1200	2800	2250	1682
$(L/D)_{Cruise}$			16.6	18.4
$(L/D)_{Ingress/Egress}$			10.4	19.4
S_{Wing} (m^2)			24.2	32.9
Span (m)			8.46	10.28
AR			2.96	3.21
Sea level thrust (kN)			46.6	44.32
Mission and design constraints				
$L_{Take\text{-}off}$ (m)		1500	1102	460
$L_{Landing}$ (m)		1500	1513	1448
Specific E. power (m/s)	60		69	67.9
Acceleration time (s)		40	35	37
Nose-on RCS (dBsm)		− 20	− 27.8	− 25.3
Static margin (%)	− 15	15	$-16.6_{(min)}$	$-13.6_{(min)}$
			$-1.5_{(max)}$	$21.2_{(max)}$

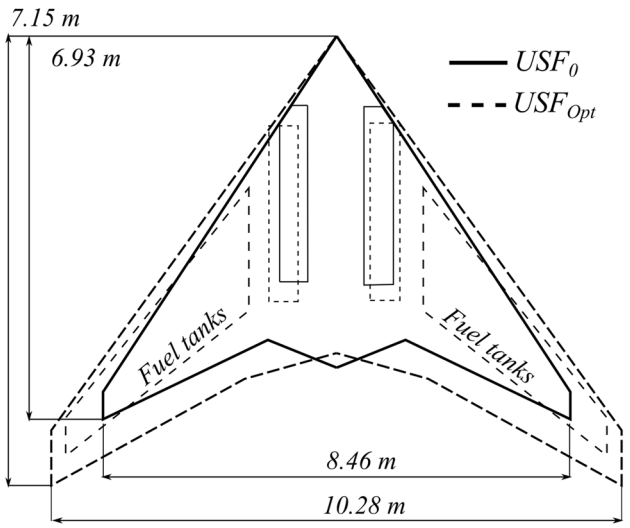


Fig. 13 Top view comparison between design starting point and optimised design

POFACETS code, with excellent agreement of results between platforms.

Finally, a lambda-wing unmanned strike fighter UCAV configuration has been designed following AIAA's unmanned strike fighter RFP. The GENUS framework UCAV modules are applied to improving the initial design point to comply with the mission requirements. A significant improvement in aerodynamic performance is shown, as well as a take-off mass reduction of 8% and a fuel mass reduction of 25%.

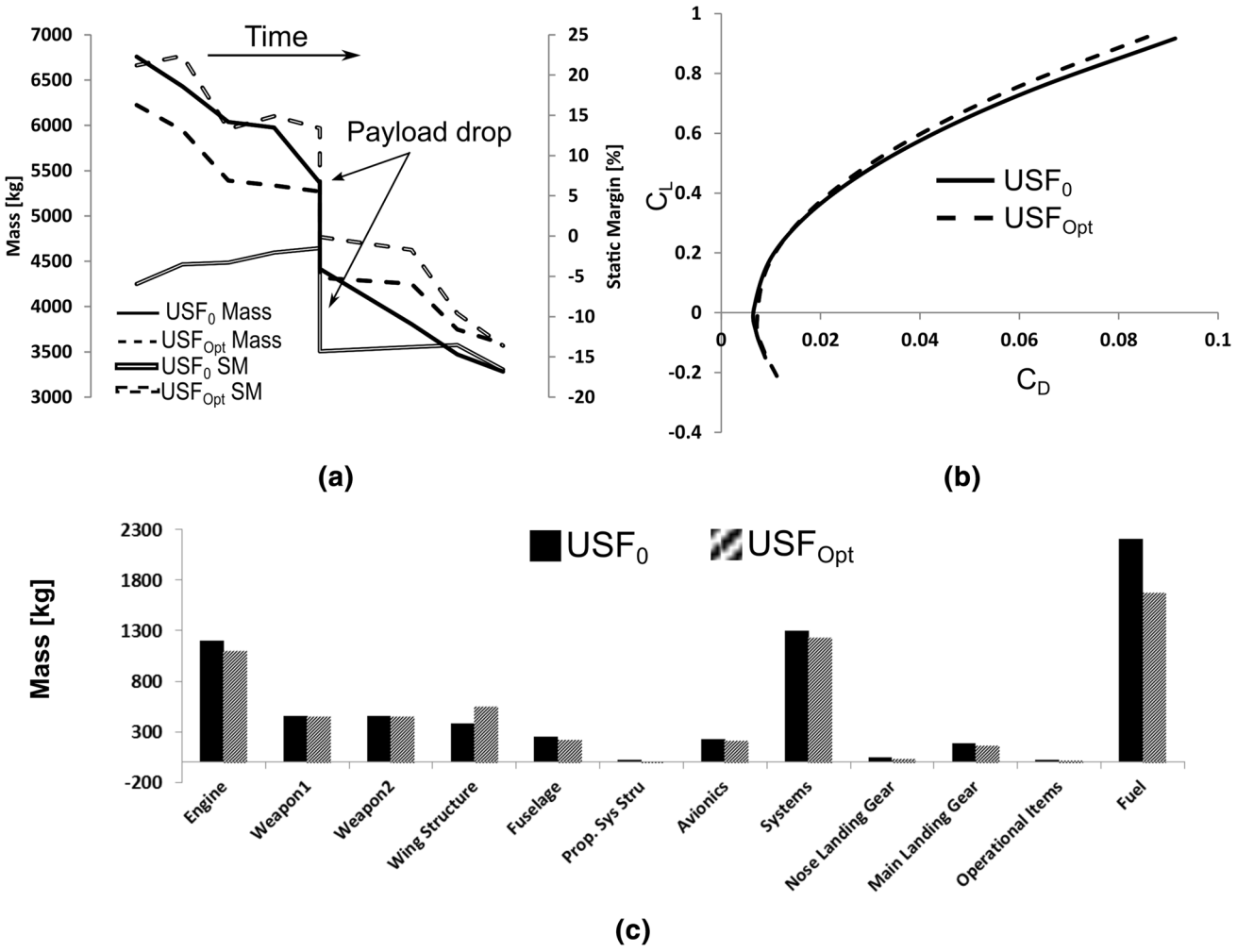


Fig. 14 Mass and static margin profiles (**a**), drag polar $M = 0.7$ (**b**), and mass breakdown (**c**)

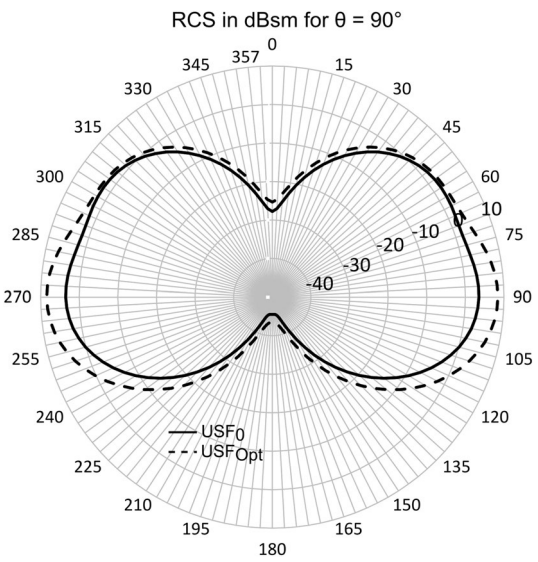


Fig. 15 RCS signature comparison

Acknowledgements The authors would like to acknowledge the contributions of Mr. Yicheng Sun to the aerodynamics, propulsion, and stability modules.

Compliance with ethical standards

Conflict of interest The authors declare that they have no conflict of interest.

Open Access This article is distributed under the terms of the Creative Commons Attribution 4.0 International License (http://creativecommons.org/licenses/by/4.0/), which permits unrestricted use, distribution, and reproduction in any medium, provided you give appropriate credit to the original author(s) and the source, provide a link to the Creative Commons license, and indicate if changes were made.

References

1. Martins, J.R.R.A., Arbor, A.: Multidisciplinary design optimization: a survey of architectures. AIAA J. **51**, 2049–2075 (2013). https://doi.org/10.2514/1.J051895
2. Kesseler, E., Guenov, M.D., Lu, F.K. (eds.) Advances in Collaborative Civil Aeronautical Multidisciplinary Design Optimization. Progress in Astronautics and Aeronautics. American Institute of Aeronautics and Astronautics, Reston (2010)
3. Howe, D.: Aircraft Conceptual Design Synthesis. Professional Engineering Publishing Limited, London (2000)
4. Roskam, J.: Airplane Design. Roskam Aviation and Engineering Corporation, Ottawa (1985)
5. Raymer, D.P.: Aircraft Design: A Conceptual Approach, 2nd edn. In: Przemieniecki, J. (ed.) AIAA, Washington D.C. (1992)
6. Nguyen, N.-V., Choi, S.-M., Kim, W.-S., Lee, J.-W., Kim, S., Neufeld, D., et al.: Multidisciplinary unmanned combat air vehicle system design using multi-fidelity model. Aerosp. Sci. Technol. Elsevier Masson SAS. **26**(1), 200–210 (2013). https://doi.org/10.1016/j.ast.2012.04.004
7. Tomac, M., Rizzi, A., Nangia, R.K., Mendenhall, M.R., Perkins, S.C.: Engineering methods applied to an unmanned combat air vehicle configuration. J. Aircr. **49**(6), 1610–1618 (2012). https://doi.org/10.2514/1.C031384
8. Woolvin, S.J.: A conceptual design study of the 1303 UCAV configuration, AIAA 2006–2991. 24th Applied Aerodynamics Conference. San Francisco, California, 5–8 June, AIAA, Reston, VA (2006)
9. Tyan, M., Nguyen, N., Lee, J.-W.A. Van, Tailless, U.A.V., Multidisciplinary design optimization using global variable fidelity modeling. Int. J. Aeronaut. Sp. Sci. **18**(4), 662–674 (2017). https://doi.org/10.5139/IJASS.2017.18.4.662
10. Smith, H., Sziroczák, D., Abbe, G., Okonkwo, P.: The GENUS Aircraft Conceptual Design Environment. Proceedings of the Institution of Mechanical Engineers, Part G: Journal of Aerospace Engineering. (2018). https://doi.org/10.1177/0954410018778892
11. Sun, Y., Smith, H. Turbofan airliner conceptual design in multidisciplinary design analysis optimization environment. 1st International Conference in Aerospace for Young Scientists, Beijing, P. R. China, 12–13 November. ICAYS, Beijing (2016)
12. Okonkwo, P.P.C.: Conceptual Design Methodology for Blended Wing Body Aircraft. Cranfield University, Cranfield (2016)
13. Sziroczák, D.: Conceptual Design Methodologies Appropriate to Hypersonic Space and Global Transportation Systems. Cranfield University, Cranfield (2015)
14. Abbe, G., Smith, H.: Technological development trends in solar-powered aircraft systems. Renew. Sustain. Energy Rev. **60**, 770–783 (2016). https://doi.org/10.1016/j.rser.2016.01.053
15. Sun, Y., Smith, H. Supersonic business jet conceptual design in a multidisciplinary design analysis optimization environment. AIAA/ASCE/AHS/ASC Structures, Structural Dynamics, and Materials Conference, 8–12 Jan, Kissimmee, Florida. AIAA, Reston (2018). https://doi.org/10.2514/62018-1651
16. Sepulveda, E., Smith, H.: Technology challenges of stealth unmanned combat aerial vehicles. Aeronaut. J. **121**(1243), 1261–1295 (2017). https://doi.org/10.1017/aer.2017.53
17. Craidon, C.B.: A description of the Langley Wirefram Geometry Standard (LaWGS) format. Langley, Virginia (1985)
18. NASA Glenn Research Center. EngineSim Version 1.8a. EngineSim (2015). https://www.grc.nasa.gov/WWW/k-12/airplane/ngnsim.html. Accessed 23 June 2017
19. Hendricks, E.S., Falck, R.D., Gray, J.S.: Simultaneous propulsion system and trajectory optimization. 18th AIAA/ISSMO Multidisciplinary Analysis and Optimization Conference. American Institute of Aeronautics and Astronautics (2017). https://doi.org/10.2514/6.2017-4435
20. Gundlach, J.: Designing Unmanned Aircraft Systems - A Comprehensive Approach, 1st edn. American Institute of Aeronautics and Astronautics, Reston, VA (2012)
21. Roskam, J.. Airplane Design Part V: Component Weight Estimation. Airplane Design. Roskam Aviation and Engineering Corporation, Ottawa (1985)
22. Cranfield College of Aeronautics. Aircraft Mass Prediction—DAet 9317 and DAet 9318. Cranfield University, Cranfield
23. Virginia Tech. Program Friction. http://www.dept.aoe.vt.edu/~mason/Mason_f/FRICTman.pdf. Accessed 19 Oct 2017
24. Gur, O., Mason, W.H., Schetz, J.: Full-configuration drag estimation. J. Aircr. **47**(4), 1356–1367 (2010). https://doi.org/10.2514/1.47557
25. Carmichael, R., PAN AIR: Public Domain Aeronautical Software (PDAS) (2015). http://www.pdas.com/panair.html. Accessed 24 Apr 2017
26. Sidwell, K.W., Baruah, P.K., Bussoletti, J.E., Medan, R.T., Conner, R.S., Purdon, D.J., PAN AIR: A computer program for predicting subsonic or supersonic linear potential flows about arbitrary configurations using a higher order panel method. NASA CR-3252. Volume II—User's Manual (Version 3.0). Seattle, Washington; March (1990)
27. Capone, F.J.: Wind Tunnel/Flight Data Correlation for the Boeing 737-100 Transport Airplane. NASA TM X-72715. Hampton, Virginia; August (1975)
28. McParlin, S.C., Bruce, R.J., Hepworth, A.G., Rae, A.J.: Low speed wind tunnel tests on the 1303 UCAV concept, AIAA 2006–2985. 24th Applied Aerodynamics Conference. San Francisco, California 5–8 June. AIAA, Reston (2006)
29. Harris, R.V.J.: An Analysis and Correlation of Aircraft Wave Drag, NASA TM X-947. Langley, Virginia (1964)
30. Lynn, S., Pete, M. takeoff2.c. Virginia Tech, Blacksburg (1994). http://www.dept.aoe.vt.edu/~mason/Mason_f/MRsoft.html#TakeOff. Accessed 20 February 2018
31. Brandt, S., Stiles, R.J., Berin, J.J., Whitford, R.: Introduction to Aeronautics: A Design Perspective, 2nd edn. Shetz, J.A. (ed.) American Institute of Aeronautics and Astronautics, Reston, (2004)
32. ESDU. Energy HEIGHT Method for Flight Path Optimisation—ESDU 91016. September (1991)
33. Gudmundsson, S.: General Aviation Aircraft Design: Applied Methods and Procedures, 1st edn. Butterworth-Heinemann, Oxford (2014)
34. de Castro, H.V.: The Longitudinal Static Stability of Tailless Aircraft. CU/COA-2000/0018/1. Cranfield (2000)
35. Elking, D.M., Roedder, J.M., Car, D.D., Alspach, S.D.: A review of high-frequency radar cross section analysis capabilities at McDonnell Douglas aerospace. IEEE Antennas Propag. Mag. **37**(5), 33–43 (1995)
36. Garrido, E.J.: Graphical User Interface For A Physical Optics Radar Cross Section Prediction Code. Naval Postgraduate School, Monterey (2000)
37. Chatzigeorgiadis, F.: Development of Code for a Physical Optics Radar Cross Section Prediction and Analysis Application. Naval Postgraduate School, Monterey (2004)
38. Lloyd, J.E.. QuickHull3D (2004). https://www.cs.ubc.ca/~lloyd/java/quickhull3d.html. Accesed 18 March 2017
39. AIAA. Draft from the AIAA Unmanned Strike Fighter RFP for AIAA Team Student Design Competition. http://www.dept.aoe.vt.edu/~mason/Mason_f/SD1RFP.pdf. Accesed 18 January 2018



https://dspace.org/

Multidisciplinary analysis of subsonic stealth unmanned combat aerial vehicles

Sepulveda, Eduardo; Smith, Howard; Sziroczak, David

2018-08-01
Springer
https://doi.org/10.1007/s13272-018-0325-0
Sepulveda E, Smith H, Sziroczak D. (2019) Multidisciplinary analysis of subsonic stealth unmanned combat aerial vehicles. CEAS Aeronautical Journal, Volume 10, Issue 2, June 2019, pp. 431-442

Downloaded from a DSpace repository. https://dspace.org/